Applied Materials Today 20 (2020) 100651

Contents lists available at ScienceDirect

Applied Materials Today

journal homepage: www.elsevier.com/locate/apmt

# Micro-nano hybrid-structured conductive film with ultrawide range pressure-sensitivity and bioelectrical acquirability for ubiquitous wearable applications

Lijuan Zhang[a], Xu Liu[a], Mengjuan Zhong[a], Yaning Zhou[a], Yangjian Wang[a], Tianhao Yu[a], Xiaobing Xu[a], Wei Shen[a], Lu Yang[a], Nan Liu[b], Di Wei[a,*], Zhongfan Liu[c,*]

[a] Beijing Graphene Institute, Beijing 100094, PR China
[b] Beijing Key Laboratory of Energy Conversion and Storage Materials, College of Chemistry, Beijing Normal University, 100875, PR China
[c] Center for Nanochemistry, Beijing Science and Engineering Center for Nanocarbons, Beijing National Laboratory for Molecular Sciences, College of Chemistry and Molecular Engineering, Peking University, Beijing 100871, PR China

ARTICLE INFO

*Article history:*
Received 9 January 2020
Revised 9 March 2020
Accepted 30 March 2020

*Keyword:*
Flexible pressure sensor
Wide sensing range
Stretchable dry electrodes
Health care
Wearable electronics

ABSTRACT

Flexible and multifunctional sensing materials have emerged as a new class of prospective components for various practical wearable applications. Here, a micro-nano hybrid-structured conductive film (HCF) incorporating 1D carbon fibers and 0D carbon nanoparticles (CNPs) into polydimethylsiloxane matrix, presents remarkable pressure-sensitivity and bioelectrical acquirability. The HCF sensor exhibits a superior sensitivity of 43.15 $kPa^{-1}$ over a broad pressure range from 2.5 Pa to 200 kPa, keeping a considerable sensitivity of 7.28 $kPa^{-1}$ up to 800 kPa. The devices are demonstrated in monitoring artery pulses, swallowing, acoustic vibrations, gestures and human body motions. Furthermore, benefiting from the exceptionally high conductivity and tailorability in different shape structures, the HCF could also function as stretchable dry electrodes, which can be conformal contact with skin for acquiring high-quality bioelectrical signals including electrocardiogram (ECG), electromyogram (EMG) and electrooculogram (EOG). The attainment of both excellent pressure sensing performance and bioelectrical acquirability of HCF, potentially initiates vast applications in wearable electronics.



## 1. Introduction

In recent years, wearable electronic devices have attracted lots of interests for their potential applications including robot sensors, health care and motions monitoring etc. [1-7]. The advantages of the thin geometric structure, lightweight, flexibility with pretty high sensitivities enable them to be integrated onto curved surfaces and *in situ* monitor vital signals, such as wrist pulse, [8,9] respiration, [10] blood pressure, [11] body motion, [3] mechanical vibration, [12,13] and even bioelectrical signals, [14-17] etc.

Conductive elastomers as multifunctional filler-matrix materials together with diverse sensing performances are considered as essential components for wearable electronics [17-20]. Polydimethylsiloxane (PDMS) is a silicon-based elastomer, which is one of the most popular materials in flexible devices because of its biocompatibility, wear comfortability, optical transparency, water resistance, and low fabrication cost [21-23]. Conductive PDMS-based composites can be achieved by adding conductive fillers such as metal particles, [24-26] metal nanowires, [27] and conductive carbon materials [21,23,28]. Among them, carbon materials including carbon black (CB), carbon nanotubes (CNTs), graphene and carbon fibers (CFs) have been reported as ideal conductive fillers due to their prominent features of lightweight, chemical stability, and excellent electrical conductivity. Hence, carbon-based PDMS composites show various applications in the field of flexible electronics, such as pressure sensors, bioelectrical transducers, and temperature detectors, etc. [5,29-32].

It is well known that flexible pressure sensors can be classified into resistive, [33,34] capacitive [35,36] and piezoelectric [37] types, based on different sensing elements and mechanisms. The resistive-type pressure sensors operating on the principle of converting external force into electrical signals are used extensively due to the advantages of simple fabrication procedures, low power consumption, prompt response, excellent stability, convenient signal acquisition and cost effectiveness. [1,38,39] The carbon-based PDMS composites as sensing materials have attracted lots of interests in resistive-type pressure sensors. As an example, Pan et al. [40] reported a pressure sensor based on carbon nanotube-liquid crystal-PDMS composites, which showed a sensing range of 0-80

* Corresponding authors.
*E-mail addresses:* diwei@hotmail.com (D. Wei), zfliu@pku.edu.cn (Z. Liu).

https://doi.org/10.1016/j.apmt.2020.100651
2352-9407/

kPa with a sensitivity of 5.35 $kPa^{-1}$. In another work reported by Wang et al., [18] a carbonized lignin pressure sensor possessed a relatively wide pressure range from 0 to 130 kPa. It only presented high sensitivity up to 57 $kPa^{-1}$ in the low-pressure region of 0-0.5 kPa. However, the sensitivity decreased to 1.08 $kPa^{-1}$ beyond 3 kPa, which seriously confined its use in the high-pressure region. Some hierarchical resistive pressure sensors were developed to promote sensing performance by fabricating external patterns or inner porous structures. For instance, Sun et al. [5] demonstrated a pressure sensor consisting of hierarchical graphite/PDMS composites, revealing a high sensitivity of 64.3 $kPa^{-1}$ in the low-pressure region of 0-1 kPa and keeping 12.4 $kPa^{-1}$ in the region of 1-10 kPa. Surface patterned conductive graphite/PDMS foams were also prepared, exhibiting superior sensitivities of 245 and 90 $kPa^{-1}$ in 0-120 and 120-150 kPa, respectively. The hierarchical structure improved the sensitivity of the sensor obviously, but offered no significant help to further expand the sensing range. Attaining superior sensitivity and ultrawide pressure range is still a daunting challenge. Generally speaking, the resistive-type pressure sensor consisting of carbon-based PDMS composites demonstrates high sensitivity over fairly wide measuring range for various wearable applications.

Moreover, the conductive carbon-based PDMS composites can be also used as dry electrodes to capture bioelectrical signals, due to the flexibility and biocompatibility. For example, Jung and co-workers [41] fabricated CNTs/PDMS composite as flexible dry electrodes, which exhibited a long-term ECG monitoring capability and robustness to motion and sweat. Chlaihawi et al. [42] developed flexible dry electrodes by coating multi-walled carbon nanotube (MWCNT)/PDMS composite on screen printed electrode for ECG monitoring. Reyes et al. [43] demonstrated hydrophobic electrodes comprised of CB and PDMS for underwater ECG monitoring. These literatures proved the conductive carbon-based PDMS composites as dry electrodes can adhere to the skin steadily for long-term bioelectrical monitoring. However, the resistance of conductive carbon-based PDMS composites changes during the skin stretching, affecting the accuracy of bioelectrical signals. Fortunately, structure design for stretchable network has evolved to decrease the local stress and strain of thin-film materials. For instance, Xu et al. [44] developed a metal sensor in an interwoven serpentine morphology for EMG monitoring. Then the research group further developed an Au fractal electrode conformal contact with the cardiac surface to acquire ECG signals [45]. These structure designs could improve the stretchability and conformality of thin-film materials. Therefore, purposeful structure design of dry electrodes made of conductive elastomer provides good solution to avoid resistance change due to deformation and guarantee signal accuracy. The conductive carbon-based PDMS composites reported in this paper can be used in both pressure sensors and dry electrodes, demonstrating great potential for ubiquitous wearable electronics.

A novel hybrid-structured conductive film (HCF) consisting of 1D CFs and 0D CNPs from the conductive carbon ink (CCI) is reported in this paper. These two kinds of conductive fillers were employed to form electronic conductive networks in PDMS matrix, which produced continuously change in resistance when the applied force increases constantly to a very high load. The HCF pressure sensor exhibited a low detection limit of 2.5 Pa and quite wide working range up to 800 kPa. A high sensitivity of 43.15 $kPa^{-1}$ was achieved over 2.5 Pa to 200 kPa and it still maintained 7.28 $kPa^{-1}$ at the high-pressure range of 500-800 kPa, which exceeded most of the results reported in literatures [2,3,5,46]. With a view of real-world applications, our sensors were expected to play an important role in various demonstrations at a broad pressure-sensing range, such as artery pulses, human motions, and the pressure between tires and ground as vehicles running over. Meanwhile, due to the high conductivity and tailorability, the HCF was cut into serpentine network to conformal contact with skin and functioned as stretchable dry electrodes to obtain high-quality bioelectrical signals. The versatile HCF shows the potential to open promising opportunities in various fields including real-time all-around healthcare monitoring, human-machine interfaces, and even industrial scenarios.

## 2. Results and discussion

The HCF can be potentially made into mass production with outstanding flexibility, as presented in Fig. 1a. It can be used as pressure sensing layers or electrodes to monitor the viral artery pulses, swallowing, acoustic vibrations, gestures, body motions, and bioelectrical signals (Fig. 1b, c). A simple method has been investigated in the preparation of HCF (Fig. S1), and the details are described in the experimental section. Fig. 1d indicates the conducting and pressure sensing mechanism of HCF. CFs set up a skeleton in the PDMS matrix, and CNPs from CCI distribute in the inter-space inside CFs skeleton and the surfaces of CFs, as shown in Fig. S2. It is notable that CFs provide long-range charge transport channel, while the CNPs are responsible for short-range charge transport. The two fillers integrate conductive paths via complete physical contacts and incomplete contacts which establishes a tunneling resistance for an electron flow in the HCF [47]. The multistage and synergistic conductive network is beneficial to improve electrical conductivity of HCF. This conductive network possesses excellent pressure-sensing performance. When an external force is applied, the effective conductive network consisting of the physical contact and the tunneling resistance between fillers is formed. The gaps between fillers change to form the physical contact and tunneling resistance, as shown in Fig. S3, resulting high sensing sensitivity [48].

Apparently, the concentrations of CFs and CCI in the PDMS matrix are critical aspects to determine the electrical conductivity and pressure sensitivity. Table S1 illustrates the change in sheet resistances of HCF with different concentrations of fillers. It is obvious that the sheet resistances decrease with increasing one filler while keeping another constant. Increasing in concentrations of CFs (10, 15, and 20 wt.% in CFs/PDMS) and CCI (31 to 35 wt.% in CFs/CCI/PDMS) provide more stable and denser conductive skeleton and more conductive paths. It is clearly observed that the sheet resistance reduces to 43.79 Ω/sq when the concentrations are 20 wt.% CFs and 35 wt.% CCI, named as $HCF_{20/35}$ (the HCF of other concentrations were named by this way). As following, the pressure sensitive HCFs were further tested and studied. Fig. 2 demonstrates the relationship between current variation ratios ($\Delta I/I_0$, here $\Delta I$ is the measured change in current, and $I_0$ denotes the measured current without loading) and the applied pressure. The sensitivity (S) of the pressure sensors is defined as $S=\delta(\Delta I/I_0)/\delta P$. HCFs function as pressure sensing layers achieving a pretty wide range of 0-800 kPa, and the sensitivity are divided into three linear regions of 0-200 kPa, 200-500 kPa, and 500-800 kPa. Fig. 2a illustrates the pressure sensing performance is improved with increasing content of CFs while keeping the CCI constant. It is verified that 20 wt.% CFs is the best concentration for pressure sensitivity. Then, keeping the content of CFs constant, the sensing property is measured further to change the content of CCI. Fig. 2b shows the $HCF_{20/35}$ exhibits the best sensing performance, which are 43.15 $kPa^{-1}$, 13.69 $kPa^{-1}$, and 7.28 $kPa^{-1}$ in these three pressure regions. Hence, the $HCF_{20/35}$ was chosen as the optimum proportion in the following tests.

The mechanical property of $HCF_{20/35}$ is measured by tensile test. The introduction of the two fillers into PDMS lowers the tensile breaking strain and increases modulus comparing with the pure PDMS (Fig. S4). These property changes are attributed to the

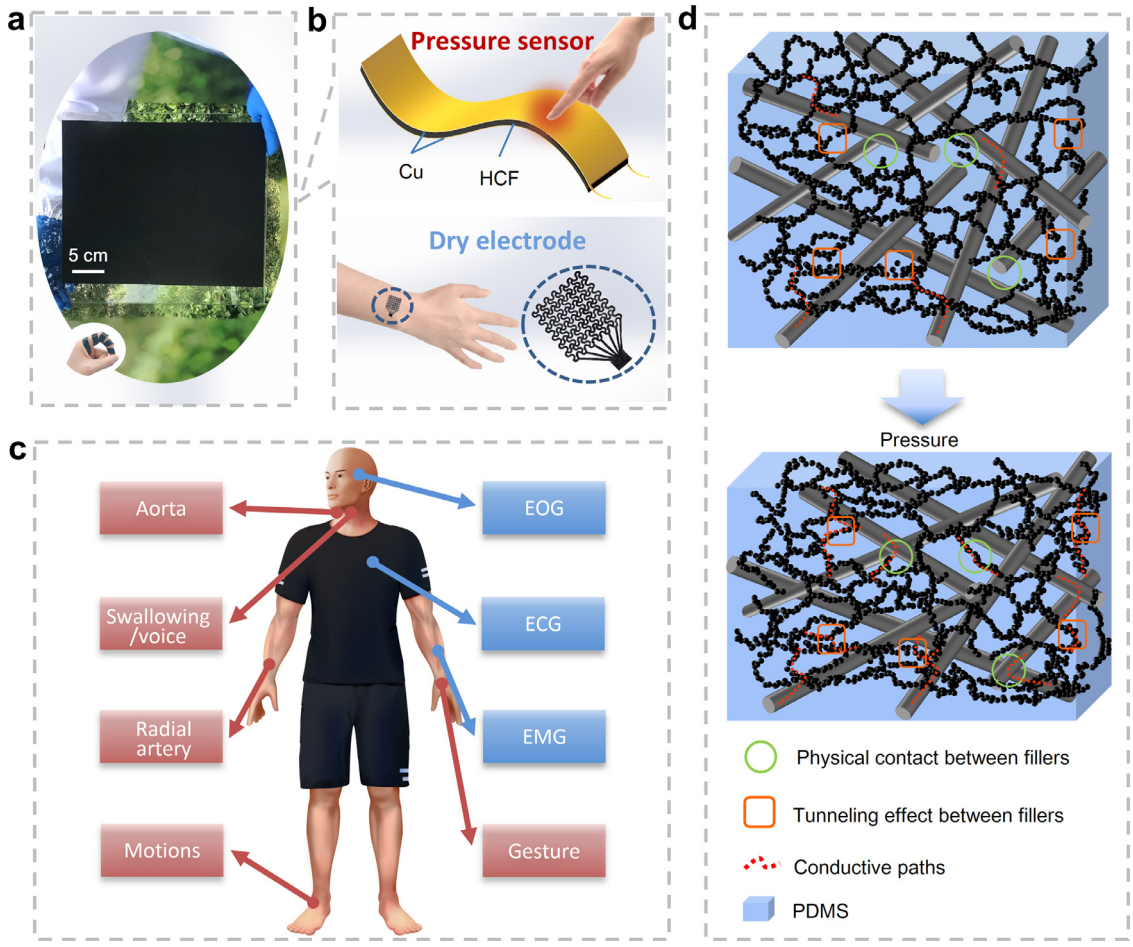


**Fig. 1.** (a) Photography of HCF. (b) Schematic of a flexible pressure sensor and a stretchable electrode. (c) Schematic illustration of the pressure sensors and stretchable dry electrodes for monitoring human vital signs. (d) Scheme of micro-structure change in the HCF with pressure applied.

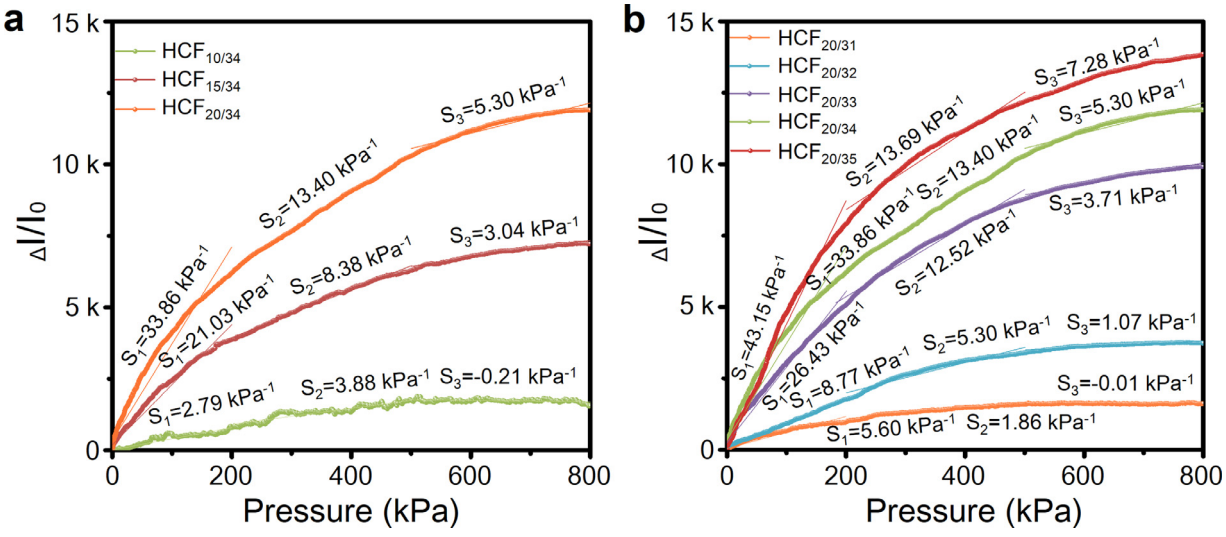


**Fig. 2.** Current responses of the sensor based on different radio of CFs (a) and CCI (b) to continuous pressure from 0 to 800 kPa.

hydrodynamic effect arising from the in-clusion of rigid particles and an increase in the cross-linking density created by polymer filler interactions [49]. The Young's modulus of PDMS is 1.50 MPa. The CF/PDMS and CCI/PDMS show higher modulus of 7.06 and 4.37 MPa, respectively, benefiting from the CF and carbon nanoparticles in CCI working as reinforced fillers. This may be demonstrated that increasing the aspect ratio of the filler increases the modulus [21]. The $HCF_{20/35}$ presents highest Young's modulus of 14.61 MPa resulted from the synergetic reinforcement of CF and CNPs. Meanwhile, the resistance change of $HCF_{20/35}$ with increasing strain is measured, as shown in Fig. S5. The result shows that the normalized current change was lower than 100% even at 50% strain,

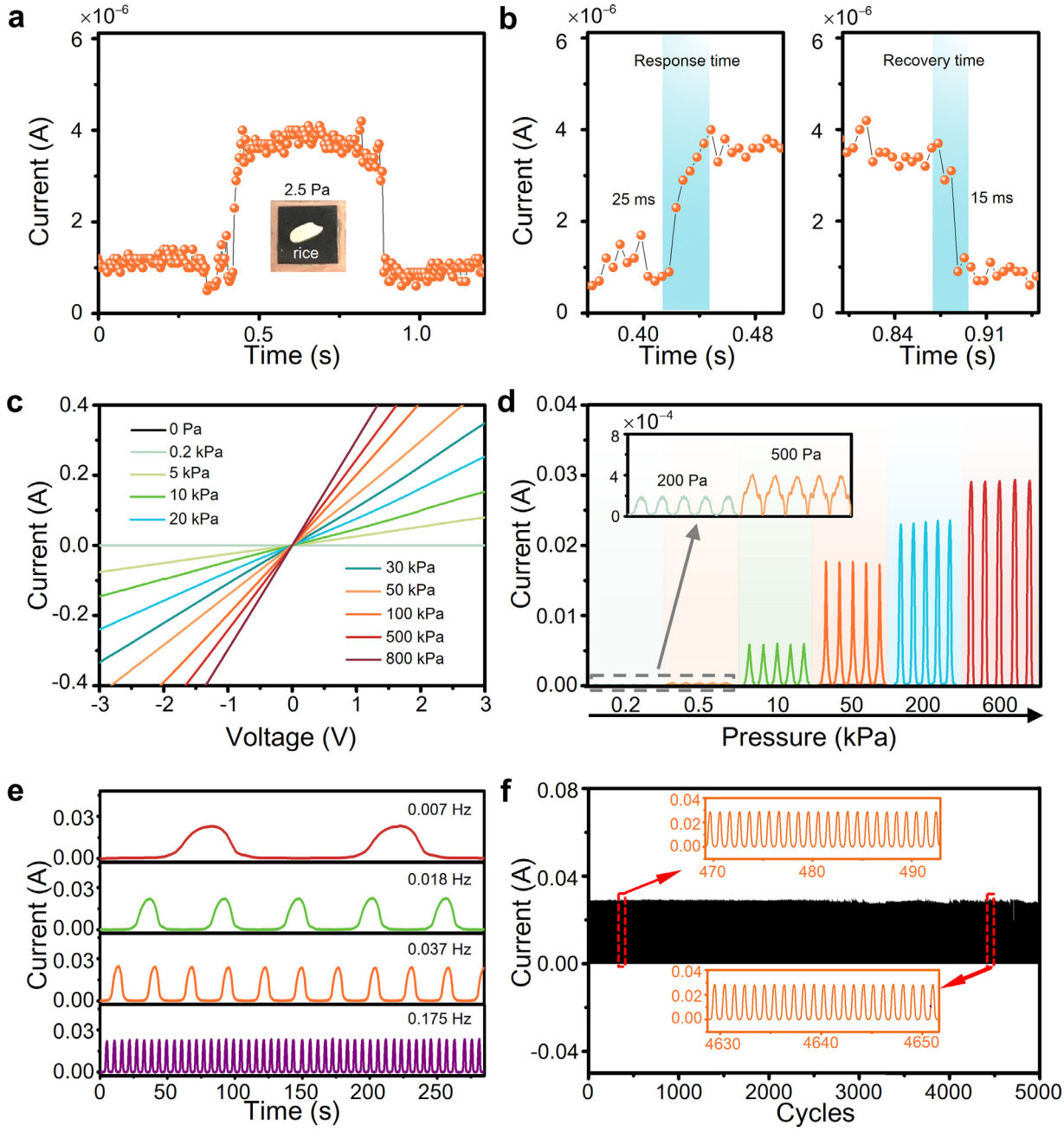


**Fig. 3.** Sensing performance of the $HCF_{20/35}$ sensors. (a) Current responses to loading/unloading a grain of rice (25 mg) on the sensor. (b) Response time and recovery time of the sensor estimated from (a). (c) The I-V curves of the sensor under the pressure from 0 to 800 kPa. (d) Cyclic current responses of the sensor to different pressures. (e) Cyclic current responses of the sensor to 200 kPa at different frequencies. (f) Stability and durability of the sensor over 5000 loading/unloading cycles at a pressure of 200 kPa.

meaning that the $HCF_{20/35}$ thin films was more suitable for stretchable conductive films other than strain sensor [47].

The $HCF_{20/35}$ consisting of two fillers and PDMS has shown high sensitivity and wide sensing range as pressure sensor. However, it is necessary to know the sensing property of this material when the PDMS filled only with carbon fibers, or PDMS filled only with CCI. Fig. S6a and Fig. S6b exhibit the cross section morphologies of CF/PDMS composite and CCI/PDMS composite. It is obvious that the carbon fibers are dispersed in PDMS matrix. It is difficult to find carbon nanoparticles in the SEM image due to smaller particle size. Fig. S6c displays the sensitivity curve of both at 0 to 800 kPa pressure. The results imply that only carbon fibers as filler is difficult to integrate the conductive path at the mass ratio in PDMS matrix even under high pressure, due to the large distance between adjacent CFs. Besides the composite only with carbon particles presents a subtle and unstable conductivity changes with increasing pressure. This advantage owes more to the effective electron tunneling occurring at a small and proper inter-particle distance under the compressive state. The carbon fibers and particles as double fillers improve the conductivity of composite material to form the effective conductive network to improve the sensor sensitivity, and this is further evidence of the synergistic effect in pressure sensing. The $HCF_{20/35}$ as pressure-sensitive layer displays a high sensitivity and a wide linearity range (Fig. 2b) for the potential applications in sensing subtle, medium and high pressures. Aiming to investigate the minimum detectable pressure of the sensor, the current response to pressure was measured by loading/unloading a grain of rice (≈25 mg), as depicted in Fig. 3a.

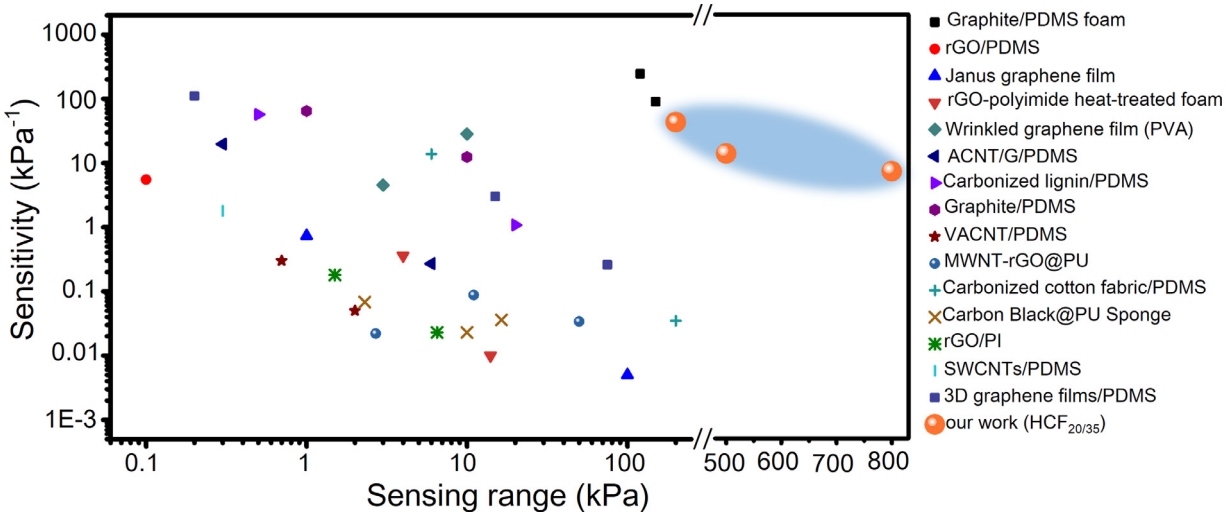


**Fig. 4.** Comparison of sensing capabilities between the current work and reported pressure sensors.

It is clearly seen that the sensor has an ultra-sensitive current response and superior sensing resolution, indicating that the sensor is capable to detect subtle pressure variations as low as 2.5 Pa. The instant sensing response time (25 ms) and recovery time (15 ms) can be observed in Fig. 3b, confirming the sensor has real-time response to the pressure. Fig. 3c presents the current-voltage (I-V) curves of the $HCF_{20/35}$ sensor from -3 to 3 V investigated at various pressure levels, implying Ohmic characteristics of the device. All the I-V curves display linear and steady responses to static pressures, and the resistance (slope of the curves) decreases corresponding to the increased applied pressure. The representative current profiles of sensor under five different applied pressures are plotted in Fig. 3d. It is notable that the good correlation between responding signals and pressure levels enable the flexible sensors to detect diverse pressure loads. As shown in Fig. 3e, current responses of $HCF_{20/35}$ sensor to constant pressure loading of 200 kPa with four loading frequencies (0.007, 0.018, 0.037, and 0.175 Hz) have been conducted. The current signals closely follow pressure loading without frequency dependence behavior. In order to confirm the durability and stability for practical applications, the $HCF_{20/35}$ sensor was subjected to multiple loading/unloading tests at 200 kPa (Fig. 3f). There is no obvious degeneration in current amplitude during whole 5000 cycles, manifesting the stability and repeatability of HCF sensor for long-term service.

Moreover, the $HCF_{20/35}$ sensor was compressed at higher pressure of 800 kPa loading/unloading 1000 cycles. The result shows the sensor has satisfying stability (Fig. S7a), benefiting from the stable conductive network structure. Fig. S7b and Fig. S7c display the cross section morphology of the material at the same area between the initial state and after 1000 cycles test, respectively. The result presents that the morphology almost no change, implying the $HCF_{20/35}$ is wearable for flexible sensors.

Fig. 4 exhibits a comparison of sensing ranges and sensitivities between current and existing pressure sensors reported in other literatures, and Table S2 presents the detail information of pressure sensors, including response time, recovery time and limitation of detection (LOD). The sensing performance depends on several crucial factors such as material properties, structures of sensing elements, substrates, and assembling of devices. Polyimide-based pressure sensors [50,51] showed lower sensitivities with limited sensing range less than 15 kPa, because of the poor ductility of polyimide. The polyurethane (PU) foams covered by MWNT-rGO ink [52] and carbon black layer [53] showed very low sensitivities because the loose porous foam structure couldn't provide dense conductive paths during loading. Sensing elements built into Janus-like surface [54] or fabric structure [55] could extend the upper limit of pressure load detection with very low sensitivities. CNTs [56], reduced graphene oxide [57], aligned carbon nanotubes/graphene (ACNT/G) [58], and 3D graphene film [59] supported by patterned PDMS substrates, presented relative high sensitivities to subtle pressure due to the micro-patterns and microstructures of sensing layers. The graphite/PDMS composite with sandpaper hierarchical microstructures [38] and further introduced porous structures [5] displayed higher sensitivities and larger sensing range, however, which still was difficult to meet the requirements of diverse application scenarios. In our current work, the $HCF_{20/35}$ sensor presented a high sensitivity of 43.15 $kPa^{-1}$ from 2.5 Pa to 200 kPa, 13.69 $kPa^{-1}$ from 200 to 500 kPa, and a considerable sensitivity of 7.28 $kPa^{-1}$ at an impressively large pressure range from 500-800 kPa. It was attributed to the elastomer matrix material and the hybrid conductive structure. PDMS as host material sustained gradual deformation over wide range of force. Moreover, two carbon materials with different dimensions as conductive fillers dispersed in elastomer matrix to form multilevel connections and synergistic conductive networks, resulting in continuous resistance decrease at the whole pressure range.

Due to the high sensitivity and wide detection range (0-800 kPa) of $HCF_{20/35}$ sensors, Fig. 5a exhibits its employment in different types of monitoring in subtle (<1 kPa), medium (1-100 kPa) and large pressure regime (>100 kPa). Pulse is an imperative physiological signal for measuring heart rate and arterial blood pressure in medical diagnosis and health monitoring. The radial pulse waves containing abundant physiological information are great significant for the diagnosis of cardiovascular diseases in clinical practice. Two $HCF_{20/35}$ pressure sensors are attached onto wrist and neck for real-time monitoring of radial and aorta arteries, respectively, as presented in Fig. 5b. From the individual wave of radial artery shown in Fig. 5c, three characteristic waves (P: shock wave, T: tidal wave and D: diastolic wave) are distinguished clearly. Then, the sensor is adhered onto throat for noninvasive monitoring muscle movements in swallowing (Fig. 5d) and acoustic vibrations (Fig. 5e). The sensor shows high sensitivity to record swallowing and differentiate various words such as "BGI", "Pressure", "Sensor" and "Hello". The visible difference between these current signals reveals a prospective capability for speech recognition devices. In order to confirm the potential applications in gesture recognition, five sensors are affixed onto lateral of knuckles to demonstrate the gestures "0, 1, 2, 3, 4, 5" (Fig. 5f). The sensors accurately capture

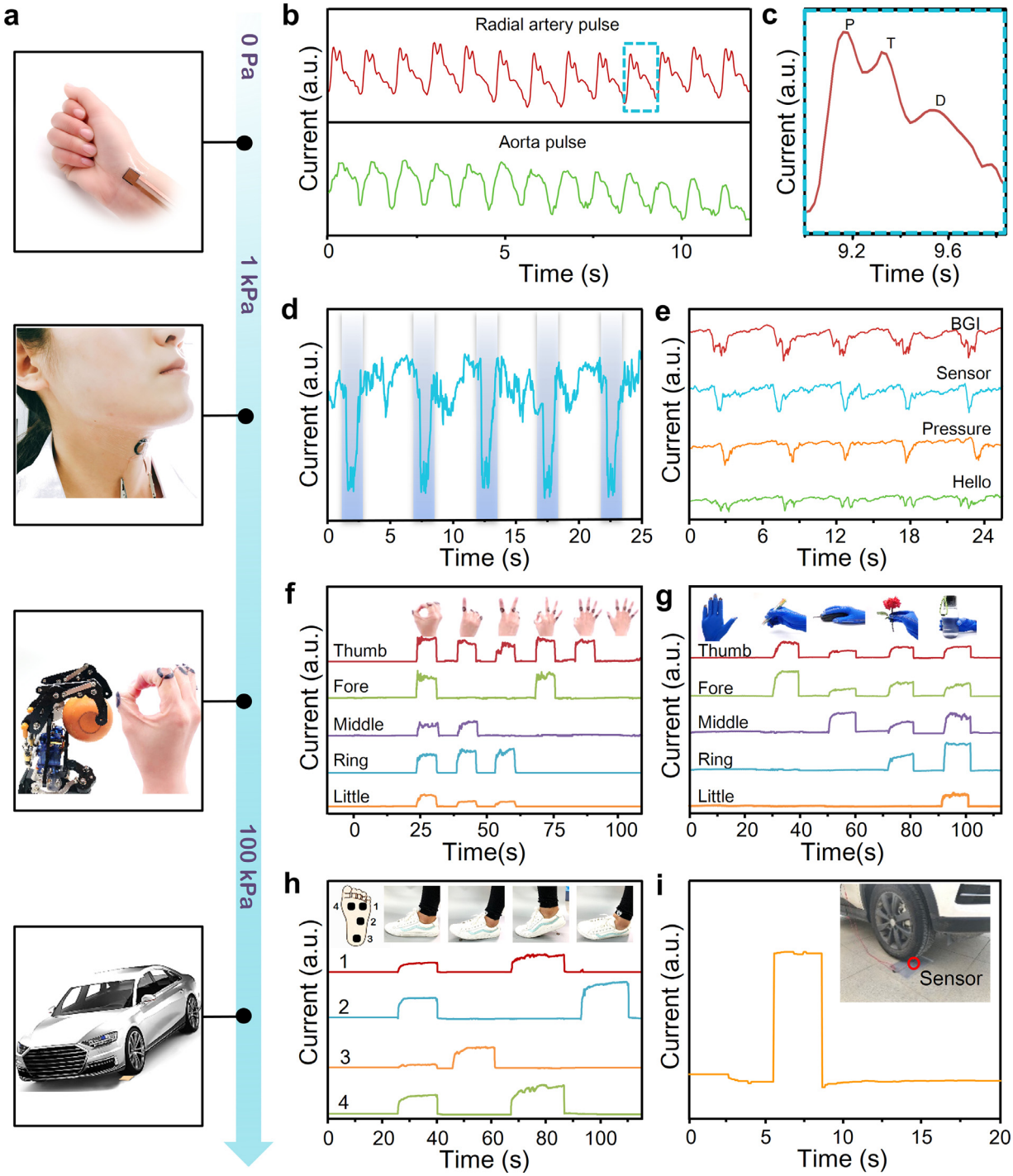


**Fig. 5.** (a) Various applications showed the highly sensitivity and large sensing range of $HCF_{20/35}$ sensors. (b) Real-time recording of arterial pulse signals of aorta and radial arteries. (c) Enlarged views in the region indicated by the dashed box in (b). (d) Measurement of swallowing. (e) Measurement of various acoustic vibrations. Current responses to various hand motions, five sensors attached on the knuckles (f) and fingertips of a rubber glove (g). (h) Current responses to different gaits. (i) High pressure applied by a car driving over the sensor.

electrical outputs from finger bending. Fig. 5g illustrates that another five sensors are attached onto fingertips to hold or grasp objects. Similarly, the current responds immediately to the pressure on fingertips. These results provide a data base for gesture recognition to distinguish different gestures and movements. Moreover, the sensor also can work as a reliable gait monitor to detect human motions. Fig. 5h indicates four pressure sensors distributed at corresponding positions on the sole in shoes, and the changes in current signals generate from the sensors with four different gaits. The sensor can also be placed under the tire of a 1.6 tons car (Fig. 5i), and it exhibits an instantaneous increase in current responds to a high pressure when the car drives over and then quickly recovers to its original state. From subtle pressure loading to large pressure levels, the $HCF_{20/35}$ sensors displayed prompt and accurate signal changes, demonstrating great potentials in wearable electronics and even in industry applications.

The $HCF_{20/35}$ material is thin, flexible, highly conductive and tailorable in the practical application as a dry electrode. The

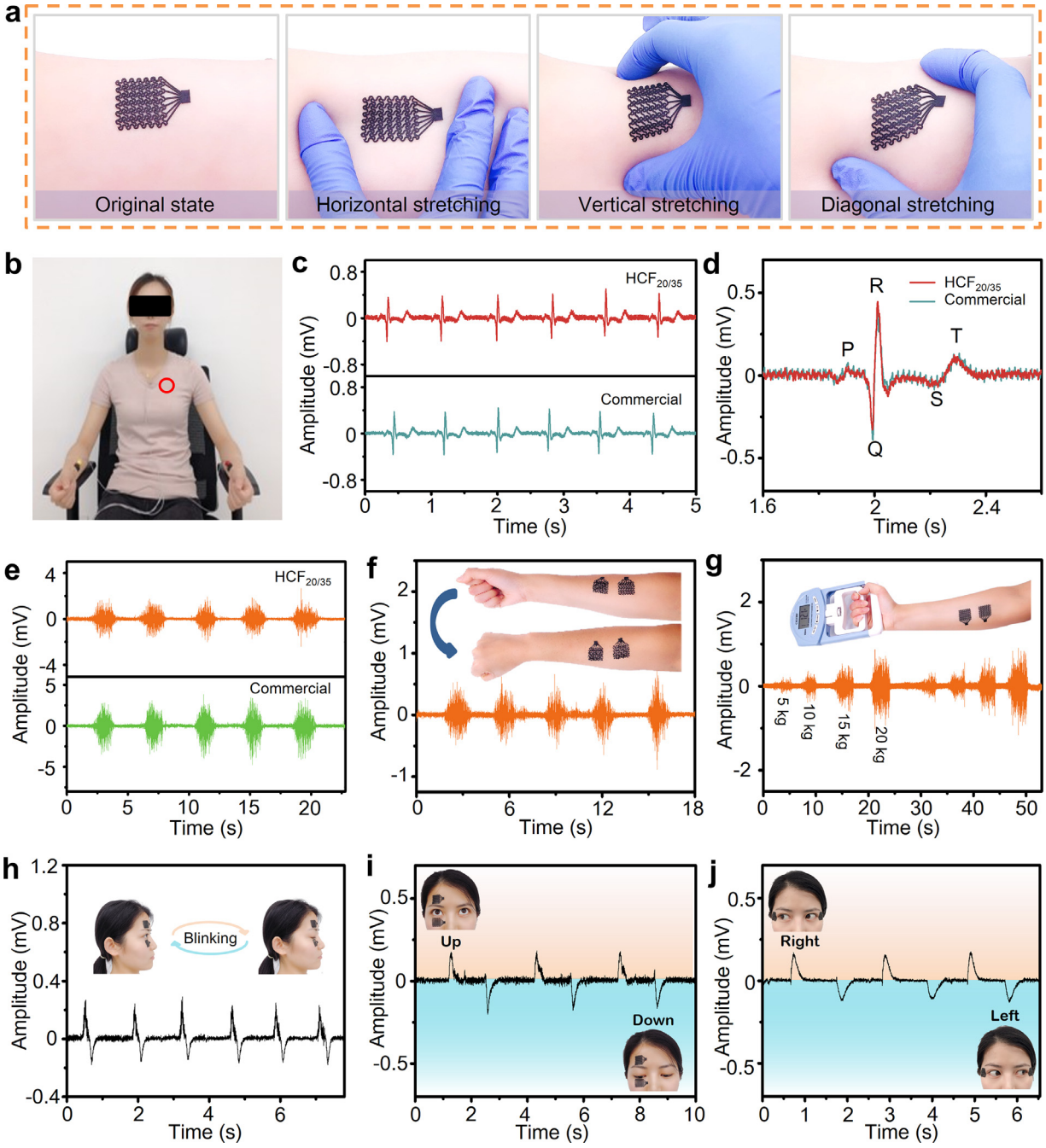


**Fig. 6.** (a) The $HCF_{20/35}$ electrodes adhered onto the surface of the skin. (b) Photograph of ECG measurement. (c) ECG signals recorded with $HCF_{20/35}$ electrodes and commercial electrodes. (d) Magnified view of the measured ECG. (e) EMG signals recorded activities of biceps brachiis with the $HCF_{20/35}$ electrodes and commercial electrodes. (f-g) EMG signals recorded activities of brachioradialis and the forearm flexors with the $HCF_{20/35}$ electrodes. (h) EOG signals of eyes blinking. (i-j) EOG signals of the eyes move horizontally and vertically.

$HCF_{20/35}$ electrode was designed with an interwoven serpentine structure to realize superior stretchability, which could be conformal with skin to acquire bioelectrical signals, such as ECG, EMG and EOG. Fig. 6a shows the stretchable $HCF_{20/35}$ electrode deforms following the skin, and it exhibits excellent conformality without constraint or delamination. For the sake of capturing ECG signals of adult (Fig. 6b), the $HCF_{20/35}$ electrodes are attached on the left and right forearms. The ECG signals are recorded clearly with identical quality comparable to commercial electrodes (Fig. 6c). Fig. 6d displays a single ECG wave, and it clearly reveals each characteristic wave, including P-wave (atrial depolarization), QRS complex (ventricular depolarization), T-wave (ventricular repolarization), and no significant baseline drifts, which are critical in routine ECG monitoring. Besides, EMG measurements are conducted by placing electrodes at biceps brachii muscle. As illustrated in Fig. 6e, compared to commercial electrodes, the $HCF_{20/35}$ electrodes reflect clear and reliable EMG signals. The electrical activity of the brachioradialis is monitored simultaneously during arm rotating (Fig. 6f). The extent of muscle contraction results changes in the amplitude of EMG signals. Hence, it is necessary to verify the accuracy of the signals through muscles stretching at different degrees. Fig. 6g clearly presents that the electrical signals of forearm flexor muscles gradually enhance with increasing in grip strength, confirming that $HCF_{20/35}$ stretchable electrodes could accurately acquire

EMG signals and could be further applied in monitoring muscular movements to adjuvant treatments for diseases or athletic injuries. Eventually, EOG detections have been investigated to verify the feasibility of stretchable $HCF_{20/35}$ electrodes. It is well known that the EOG plays an important role in testing recognitions by human-machine interfaces such as copy, read, write, browse, etc. [60] EOG signals are derived from the potentials created by the eye acting as a dipole through the positively charged cornea and negatively charged retina. [61] The potential difference between cornea and retina changes with the eyes movements. Conventional commercial electrodes, such as Ag/AgCl electrodes, cannot fit the complex surfaces around eyes due to their rigid nature, which affects the accuracy of the signal acquisition for successful human-machine interfaces. Therefore, the electrodes with excellent conformal contact to the skin and high-precision via non-invasive way are pressing need for EOG detection. The $HCF_{20/35}$ stretchable electrodes are perfectly conformal adhesion to complex curved surface of human face to capture the EOG signals. The volunteer is asked to blink her eyes at a certain frequency, and the EOG signals are observed clearly, as shown in Fig. 6h. Then, the electrodes are placed in different positions around eyes to test the horizontal eye electricity and vertical eye electricity, and the signal waves show a different variation when her eyes move left/right or up/down (Fig. 6i, j). These bioelectrical signals were obtained in the static, and some relative measurements were further carried out in motion. Fig. S8 illustrates the ECG, EMG, and EOG signals acquired by the electrodes when the subject was walking. More small interference waves appear due to the motion artifact, which is often generated from dry electrodes capturing dynamic signals. The interference waves decrease signal quality, however, the characteristic signals are clear to represent human motions. In consequence, the $HCF_{20/35}$ is cut into stretchable serpentine structure for conformal contact with the curves interfaces of human body to acquire bioelectrical signals, offering broad applications in wearable device as dry electrodes based on excellent and reliable performance.

## 3. Conclusion

In conclusion, we present a simple and efficient approach to design the micro-nano hybrid-structured conductive film (HCF) for ultrawide range pressure sensor as well as bioelectrical acquiring dry electrodes. In this HCF, the 1D carbon nanofibers and 0D CNPs as conductive fillers established multistage connections forming effective conductive networks in PDMS, greatly improved the conductivity and sensitivity of filler-matrix elastomer material. The sensor assembled by HCF exhibits an outstanding sensitivity, an extremely broad sensing range, a low limit of detection, a fast response/recovery speed, and a long-term durability in various sensing applications. The sensor allows the detection of real-time arterial pulse signals, acoustic vibrations, gestures, human body motions, and even higher pressure state. Moreover, HCF as dry electrodes, demonstrated valuable and vital applications in acquiring high-quality bioelectrical signals including ECG, EMG, and EOG etc. These results reveal the significance of combining high conductivity of pressure-sensing materials with device design to realize flexible electronics for ubiquitous wearable applications, such as health monitoring, robot sensing and human-machine interfaces. Furthermore, such 1D and 0D material design provides an efficient way to fabricate high-performance materials and could expand new materials applications in other fields.

## 4. Experimental section

### 4.1. Preparation of HCF

Carbon fibers (CFs) (diameter: 8 $\mu$m, length: 10-100 $\mu$m) (400 mesh, Haotian Nano Technology Company) and PDMS (Dow Corning Sylgard 184; the weight ratio of base to cross linker was 10:1) were mixed by a planetary centrifugal mixer (Kurabo, KK-250S) with presupposed weight ratios (10, 15 and 20 wt.% CFs in CFs/PDMS). A series of conductive carbon ink (CCI, JUJO CHEMICAL Co., Ltd) were then added into CFs/PDMS and stirred by an overhead stirrer (IKA, RW20) at 400 rpm for 3 hours. The mixture was bladed onto quartz substrates. After degassing in vacuum oven and fully curing under 100°C, the HCFs with a thickness of ~ 600 um were peeled off from quartz.

### 4.2. Characterization of thin films

SEM (10kV, FEI Quattro S) with a 10.0 kV accelerating voltage was used to characterize the morphologies of HCFs. The square resistances of HCFs were measured by four-point method (RTS-9 4-Point Probes Resistivity Measurement System, PROVES TECH).

### 4.3. Fabrication and characterization of pressure sensors

The as prepared $HCF_{20/35}$ was cut into square size (1 cm $\times$ 1 cm) and sandwiched between two copper-clad plates to complete the sensor fabrication. A mechanical performance testing system (MTS E43.104) was used to apply the pressure and a digital source meter (Keysight 2902A) was investigated to record the electrical responses of the sensors. The curves of pulse monitoring, vocal cords vibration, gesture recognition and gait monitoring demonstrations were acquired by source meter and electrochemical workstation (Metrohm, M204), respectively.

### 4.4. Measurement of mechanical property

A tensile testing machine (MTS E43.104) was employed to characterize the mechanical properties. The PDMS, CF/PDMS, CCI/PDMS and $HCF_{20/35}$ samples were tested under quasi-static tension under displacement control. The test specimens had dimensions of 33 mm (length) $\times$ 12.7 mm (width) $\times$ 0.6 mm (thickness). For the quasi-static tension test, a tensile speed of 5 mm/min was used. The electrical resistance was measured using a digital multimeter (Keysight 2902A). Thin copper wires were attached to the two ends of the specimens using a conductive silver-paste adhesive. The current change was measured by rapidly (5 mm/min) stretching the sensor to 50% strain.

### 4.5. Preparation of $HCF_{20/35}$ electrodes and measurements of bioelectrical signals

$HCF_{20/35}$ was tailored by die-cutting machine (Silhouette cameo3) with designed patterns. The bioelectrical signals ware captured by bioelectrical signal amplifier (OT Bioelettronica, quattrocento).

## Declaration of competing interest

The authors declare no conflicts of interest.

## CRediT authorship contribution statement

**Lijuan Zhang:** Conceptualization, Methodology, Writing - original draft, Writing - review & editing. **Xu Liu:** Data curation, Formal analysis, Investigation. **Mengjuan Zhong:** Data curation, Investigation. **Yaning Zhou:** Investigation, Validation. **Yangjian Wang:** Software, Validation. **Tianhao Yu:** Resources. **Xiaobing Xu:** Validation. **Wei Shen:** Resources. **Lu Yang:** Resources. **Nan Liu:** Resources, Writing - review & editing. **Di Wei:** Conceptualization, Methodology, Funding acquisition. **Zhongfan Liu:** Conceptualization, Methodology, Project administration.

## Acknowledgments

This work was supported by Beijing Municipal Science & Technology Commission No. Z181100004818004, No. Z181100001018029, and No. Z191100006119027. The authors also appreciate the technical assistance from the BGI Characterization & Quality Assurance Center.

## Supplementary materials

Supplementary material associated with this article can be found, in the online version, at doi:10.1016/j.apmt.2020.100651.

## References

[1] C. Jeong, et al., Adv. Mater. (2019) 1902689.
[2] Z. Wang, et al., Adv. Funct. Mater. 29 (11) (2019) 1807569.
[3] B. Nie, et al., Adv. Funct. Mater. 29 (22) (2019) 1808786.
[4] S. Sundaram, et al., Nature 569 (7) (2019) 698–702.
[5] Q.-J. Sun, et al., Adv. Funct. Mater. 29 (18) (2019) 1808829.
[6] C. M. Boutry, et al., Sci. Robot 3 (2018) eaau6914.
[7] B. Zhu, et al., Chem. Soc. Rev. 48 (6) (2019) 1668–1711.
[8] S. Gong, et al., Nat. Commun. 5 (2014) 3132.
[9] H. Ren, et al., ACS Nano 13 (5) (2019) 5541–5548.
[10] Y. Lee, et al., ACS Nano 12 (4) (2018) 4045–4054.
[11] S. Chen, et al., ACS Appl. Mater. Interfaces 10 (40) (2018) 34646–34654.
[12] J. Park, et al., ACS Nano 8 (5) (2014) 4689–4697.
[13] S. Chen, et al., ACS Appl. Mater. Interfaces 10 (4) (2018) 3660–3667.
[14] S. Mishra, et al., Biosens. Bioelectron. 91 (2017) 796–803.
[15] Y.J. Yun, et al., Adv. Funct. Mater. 27 (33) (2017) 1701513.
[16] S.K. Ameri, et al., ACS Nano 11 (8) (2017) 7634–7641.
[17] T. Kim, et al., ACS Nano 10 (4) (2016) 4770–4778.
[18] B. Wang, et al., J. Mater. Chem. C 6 (2018) 6423–6428.
[19] S.U. Park, et al., Adv. Mater. Technol. 3 (1) (2017) 1700158.
[20] J.-Y. Baek, et al., Sensor. Actuat. A-Phys. 143 (2) (2008) 423–429.
[21] S. Wu, et al., ACS Appl. Mater. Interfaces 9 (16) (2017) 14207–14215.
[22] K.C. Baby, et al., Resistive characterization of soft conductive PDMS membranes for sensor applications, in: 2016 IEEE Sensors Applications Symposium (SAS), Catania, Italy, 04, 2016, pp. 1–6.
[23] S. Azhari, et al., Sensor. Actuat. A-Phys. (2017) 158–165.
[24] X. Niu, et al., Adv. Mater. 19 (18) (2007) 2682–2686.
[25] M. Segev-Bar, et al., ACS Appl. Mater. Interfaces 5 (12) (2013) 5531–5541.
[26] H. Li, et al., Microelectron. Eng. 87 (2010) 1266–1269.
[27] J. Sanghyun, et al., Nat. Nanotechnol. 2 (6) (2007) 378–384.
[28] K. Beom Joon, et al., ACS Nano 6 (10) (2012) 8646–8651.
[29] N. Yogeswaran, et al., Stretchable resistive pressure sensor based on CNT-PDMS nanocomposites, in: 11th Int. Conf. on Ph.D. Res. in Microelectr. and Electr., Glasgow, United Kindom, 06, 2015, pp. 326–329.
[30] T. Yamada, et al., Nat. Nanotechnol. 6 (5) (2011) 296–301.
[31] T. Suchý, et al., Comput. Methods Biomech. Biomed. Eng. 16 (S1) (2013) 255–257.
[32] J.H. Kim, et al., Sci. Rep. 8 (1) (2018) 1375.
[33] W. Liu, et al., Small 14 (15) (2018) 1704149.
[34] S.M. Doshi, E.T. Thostenson, ACS Sens 3 (7) (2018) 1276–1282.
[35] L. Ma, et al., J. Mater. Chem. C 6 (48) (2018) 13232–13240.
[36] G.Y. Bae, et al., Adv. Mater. 30 (43) (2018) 1803388.
[37] O.Y. Kweon, et al., NPG Asia Mater. 10 (6) (2018) 540–551.
[38] Q.-J. Sun, et al., ACS Appl. Mater. Interfaces 10 (4) (2018) 4086–4094.
[39] T. Wang, et al., Chemistry 25 (25) (2019) 6378–6384.
[40] J. Pan, et al., Nanomater 8 (6) (2018) 413.
[41] H.-C. Jung, et al., IEEE Trans. Biomed. Eng. 59 (5) (2012) 1472–1479.
[42] A.A. Chlaihawi, et al., Sensing and Bio-Sensing Research 20 (2018) 9–15.
[43] B.A. Reyes, et al., Performance Evaluation of Carbon Black based Electrodes for Underwater ECG Monitoring, in: 36th Annual International Conference of the IEEE Engineering in Medicine and Biology Society (EMCB), Chicago, IL, USA, 2014, pp. 1691–1694.
[44] B. Xu, et al., Adv. Mater. 28 (22) (2016) 4462–4471.
[45] L. Xu, et al., Adv. Mater. 27 (10) (2015) 1731–1737.
[46] J. Shi, et al., Small 14 (27) (2018) e1800819.
[47] N.N. Jason, et al., J. Mater. Chem. C 5 (24) (2017) 5845–5866.
[48] N. Hu, et al., Carbon 48 (3) (2010) 680–687.
[49] L. Bokobza, Polymer 48 (17) (2007) 4907–4920.
[50] J. Yang, et al., Compos. Sci. Technol. 164 (2018) 187–194.
[51] Y. Qin, et al., ACS Nano 9 (9) (2015) 8933–8941.
[52] A. Tewari, et al., ACS Appl. Mater. Interfaces 10 (6) (2018) 5185–5195.
[53] X. Wu, et al., Adv. Funct. Mater. 26 (34) (2016) 6246–6256.
[54] Z. Song, et al., Adv. Electron. Mater. 4 (11) (2018) 1800252.
[55] L. Zhang, et al., Cellulose 26 (8) (2019) 5001–5014.
[56] X. Wang, et al., Adv. Mater. 26 (9) (2014) 1336–1342.
[57] B. Zhu, et al., Small 10 (18) (2014) 3625–3631.
[58] M. Jian, et al., Adv. Funct. Mater. 27 (9) (2017) 1606066.
[59] K. Xia, et al., Nano Res 11 (2) (2017) 1124–1134.
[60] B. Andreas, et al., IEEE T. Pattern Anal. 33 (4) (2011) 741–753.
[61] L. Tian, et al., Nat. Biomed. Eng. 3 (3) (2019) 194–205.